KSME

Springer

Journal of Mechanical Science and Technology 36 (7) 2022

Original Article
DOI 10.1007/s12206-022-0617-5

Keywords:
· Battery pack
· Passive thermal protection
· PCM
· Graphene nanoplatelets

Correspondence to:
Umit Nazli Temel
untemel@cumhuriyet.edu.tr

Citation:
Temel, U. N., Kilinc, F. (2022). The experimental and numerical investigation on thermal responses of passive thermal protected batteries in different packs from low to high discharge rates. Journal of Mechanical Science and Technology 36 (7) (2022) 3387~3398.
http://doi.org/10.1007/s12206-022-0617-5

Received November 9th, 2021
Revised February 10th, 2022
Accepted March 9th, 2022

† Recommended by Editor Chongdu Cho

The experimental and numerical investigation on thermal responses of passive thermal protected batteries in different packs from low to high discharge rates

Umit Nazli Temel and Ferhat Kilinc

Department of Mechanical Engineering, Sivas Cumhuriyet University, Sivas 58140, Turkey

Abstract This study contains experimental and numerical investigation of the shape effect of the pack on the performances of PCM (or GNP/PCM) based passive thermally protected battery packs. Also, the performances of the PCM and thermally enhanced GNP/PCM composite for battery thermal protection are compared from low to high discharge rates. The thermal response results show that the cylindrical pack performs worse than the rectangular pack in terms of the maximum temperature and maximum temperature difference performance criteria. For the maximum temperature restriction criteria, 7 % GNP/RT44 composite, that has enhanced thermal conductivity, performs better at first, but then its performance deteriorates compared to RT44 depending on the increase of its viscosity. It was determined that 7 % GNP/RT-44 extend the effective protection times by 95.8 %, 73.3 % and 28.0 % at the discharge rates of 4.4 W, 6.6 W and 8.8 W, respectively.

1. Introduction

Fossil fuel constraints, the search for more efficient systems and developing technologies are leading the traditional transport vehicles to be replaced by electric vehicles (EV) and hybrid electric vehicles (HEV). Battery packs consisting of cells connected in series and/or parallel are one of the most important power sources for the new types of vehicles such as li-ion and li-polymer. These battery cells have superior advantages such as high specific power and energy density, long cycle life, low self-discharge rate, high discharge voltage [1, 2]. However, the inner resistance of the cells and the chemical reactions that take place during their operation generates undesired heat accumulation. Especially high discharge rates cause high amount of heat generation and rapid temperature increase in the cells [3, 4]. This situation causes some negativities such as capacity fade, loss of performance, thermal imbalance and risk of explosion [5]. It is possible to overcome such negativities by using an effective thermal protection systems. Two design criteria for an ideal battery thermal protection system can be outlined as follows; i) The maximum temperature inside the battery pack should be 50 °C, ii) The maximum temperature difference inside the battery pack should be 5 °C.

The development of phase change material (PCM) based passive thermal protection systems for battery packs has become more attractive in recent years. This method works according to the principle of storing the heat generated in the battery cells as latent energy in the PCM [6]. The PCM having a high latent heat reduces the maximum temperature and the maximum temperature difference during battery pack operation [7, 8]. Solid-liquid organic PCMs are widely preferred because of their advantages such as low volume change, high latent heat, thermal and chemical stability, low cost and no toxic and corrosive effects [9]. The use of an organic PCM in battery thermal protection was first proposed by Al-Hallaj et al. [10]. But they realized that low thermal conductivity of PCM is a major drawback for passive thermal protection.

Similar studies showed that organic PCMs suffer from low thermal conductivity and cannot provide proper thermal protection for the battery thermal protection for a long run time at high discharge rates [9, 11]. It was determined that heat penetration to PCM and contact temperature of the battery cells are functions of the PCM thermal conductivity [12]. While heat penetration changes directly with the PCM thermal conductivity, battery contact temperature changes inversely. So, they are ineffective in heat dissipation for lithium-ion battery protection, and it may cause thermal runaway and even explosion [13].

One of the methods used by researchers to enhance the low thermal conductivity of organic PCMs is to make them into a PCM/fins composite. In these studies, findings have been reported that both the maximum temperature of the battery pack is reduced and the efficient use time is extended [14, 15]. The increase in system weight and/or volume and non-homogeneous temperature distribution are the main disadvantages of this method. The impregnation of PCM into metal or carbon foam pores is another solution for using thermally enhanced PCM in battery thermal protection. It has been reported that the maximum temperature of the battery pack can be reduced by 50 % in aluminum or copper foam PCM composites [16, 17]. In the last decade, expanded graphite (EG)/PCM composites have been widely preferred for battery thermal management due to their low mass, high resistance to corrosion, ease of use and avoidance of leakage problems [18, 19]. It has been determined that the EG/PCM composite has the ability to provide a homogeneous temperature distribution within the battery pack as well as maximum temperature restriction [20]. The major disadvantage of this method is that the effective protection time is short due to the limited amount of PCM to be absorbed into the foam pores. Another method for using thermally enhanced PCM in battery pack thermal protection is to homogeneously dispersion of nanoparticles with high thermal conductivity into the PCM. It has been reported that carbon-based nanoparticles effectively enhance PCM thermal conductivities than metal/metal oxide nanoparticles [21]. However, it has been reported that plate-shaped nanoparticles are more effective in thermal conductivity enhancement than nanotubes and nanofibers [22-24]. Graphene nano-platelets (GNP) are plate-shaped nanoparticles that can be used to enhance PCM thermal conductivity [25].

Some of the studies on PCM based passive thermal protection performance of battery cells have focused on determining the effects of the above mentioned enhancement methods on a single battery cell [26, 27]. In some other studies, thermal performance measurements were carried out for battery packs created by bringing together a large number of battery cells. Xu et al. [28] examined the thermal protection of cells in a cylinder package with EG/paraffin composite in terms of the composite density and paraffin fractions. They recommended that the 75 % EG/paraffin composite with a density of 890 kg/m^3 for battery thermal management. Goli et al. [29] showed that the thermal management of lithium-ion cells in a cylindrical package can be drastically improved using hybrid PCM with graphene nanofillers. They reported that the enhanced heat conduction towards the outside significantly reduced the temperature inside the lithium-ion battery package. Ling et al. [30] tested the hybrid thermal protection system consisting of PCM and forced convection on 5S4P (five cells in series and four cells in parallel) lithium-ion cells in a rectangular package. They determined that combined system prevents heat accumulation and keep the maximum temperature of the pack under 50 °C.

It was seen that the available studies focused on examining the effects of PCM or thermally enhanced PCM on the thermal protection of a single cell or a specific package. However, there is no study focusing on comparing battery pack shapes in terms of thermal protection performances. Therefore, this study primarily aims to experimentally and numerically investigate the effects of different battery pack shapes on thermal protection performance. Thereby, the effect of rectangular and cylindrical package shape on the thermal protection performances under the same conditions will be compared for the first time. Secondly, the thermal protection performances of the PCM or thermally enhanced PCM composite with high GNP mass fraction for battery thermal protection were tested from low to high discharge rates The break-even points of the protection performance based on GNP/PCM usage will be determined according to PCM based case.

2. Material and methods

2.1 Experimental details

In this study, a paraffin-based organic phase change material known as RT44 (Rubitherm Technologies, Germany) was used. It has a suitable melting temperature range (41-44 °C) for the thermal protection of battery packs. Also, for the enhancement of thermal conductivity, GNP nanoparticles (Skyspring Nanomaterials, Inc., USA) which have a surface area of 150 m^2/g and a thickness of 6-8 nm is used as supporting material. GNP/RT44 composites were prepared by adding 7 % GNP by mass into completely melted RT44 on a hot plate. After that to obtain a homogeneous dispersion, the melt mixture was subjected to an ultrasonic mixing for 30 minutes. It was observed that the addition of 7 % GNP is a mixable upper limit in the melted RT44. The thermal conductivity, differential scanning calorimetry (DSC), and viscosity characterization of the RT44 and GNP/RT44 composites was carried out using KD2 Pro (Decagon Devices. Inc., USA) and DSC-60 (Shimadzu Corporation, Japan) and rotary rheometer (Malvern Kinexus PRO, Switzerland) devices, respectively.

In this study, two representative battery packs were constructed using cylindrical electrical heaters instead of real cells. The dimensions of the heaters were chosen 18650 (18 mm in diameter and 65 mm in height) identically as the genuine cell. The battery packs were set up by mounting equally spaced electrical heaters vertically in an aluminum container. The vertical placement preference of the battery cells is due to the higher Nusselt number compared to different angles [31, 32].

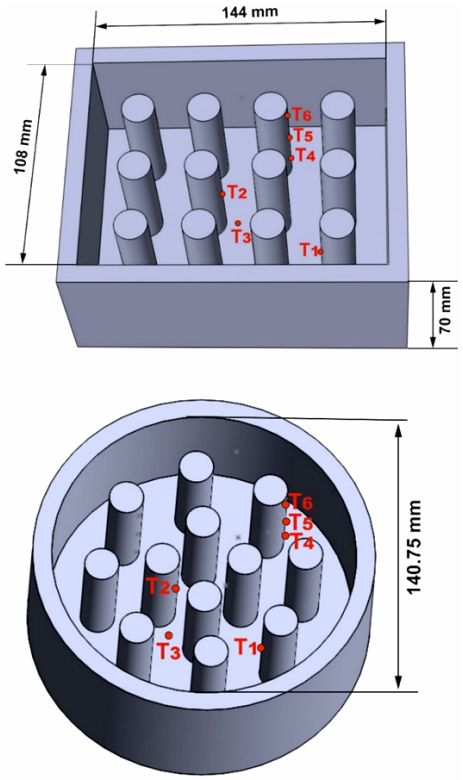

Fig. 1. The simulated battery packs.

The battery packs prepared as a cylindrical and rectangular box with an equal volume to examine the shape effect. The particular geometric properties of the battery packs were given schematically in Fig. 1. The melted RT44 or GNP/RT44 was poured into the battery packs. The battery packs were then expected to solidify at room temperature, and the heater cells were wrapped by the RT44 (or GNP/RT44). The centre-to-centre distance between the two adjacent heaters was fixed at approximately 36 mm so that the optimum GNP (or GNP/RT44) thickness of 9 mm was set for each heater [17]. The different measuring points with equivalent placement for rectangular and cylindrical battery packs are also shown in Fig. 1.

The experimental rig used in the tests consists of the battery pack, DC power supply, thermocouple connections, data collector, KD2 Pro (thermal conductivity measurement device) computer, and an air conditioning unit (Jeiotech, South Korea) (Fig. 2). The J-type thermocouples measured time-dependent temperature at specified points in the battery packs. All of the thermocouples were mounted on the half depth of the heater and named as shown in Fig. 1. At the same time, two thermocouples were connected to the upper and lower regions of one specific heater additionally to examine temperature variation throughout the heater height.

The J-type thermocouples with an accuracy of ±0.5 °C have gathered temperature data at 30 second intervals through a data collector (Agilent 34970A) and transferred it to a computer. As a representative battery cell, it is assumed that the heaters emit constant heat during the discharge process. Each heater

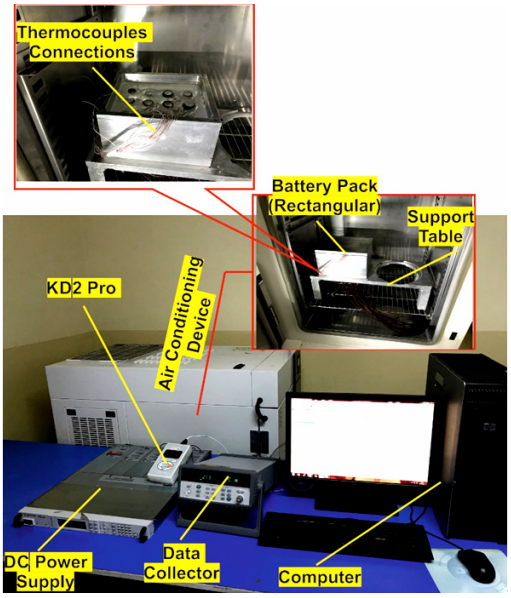

Fig. 2. Experimental test rig.

was connected to a DC power supply to emit 2.2 W, 4.4 W, 6.6 W, and 8.8 W, respectively.

Uncertainty analysis is important in terms of the precision of the measured results and the accuracy of the results obtained. To obtain the uncertainty values the following equation was used [33];

$$w_R = \left[\left(\frac{\partial R}{\partial x_1} w_1 \right)^2 + \left(\frac{\partial R}{\partial x_2} w_2 \right)^2 + \ldots + \left(\frac{\partial R}{\partial x_n} w_n \right)^2 \right]^{1/2} \quad (1)$$

where R is a function of independent variables ($x_{1,2,n}$) and resulting from the experimental study. $w_{R,1,2,n}$ can be taken as the uncertainties in the independent variables. According to the uncertainty analysis, the estimated values are ±0.5 % for type J thermocouples, ±0.2 % for the DC power supply and ±0.4 % for the measurement precision of the thermocouple of the data acquisition system (datalogger). The total uncertainty value is estimated at ±1.2 % for the whole system.

2.2 Numerical analysis

The numerical studies were conducted by using commercially available software ANSYS FLUENT 18.2 [34]. It was used to enthalpy-porosity technique to solve the melting-solidification problem. The symmetrical half 3D physical models of different packs consisting of RT44 (or 7 % GNP/RT44), and electrical heaters were created and numerically solved. The experimentally obtained characterization results of physical properties were used in numerical models. The constant heat flux for the heaters and constant heat transfer coefficient (h = 10 W/m^{2}K) for the container was applied as boundary conditions. The computational domain was divided into

2.513.276 tetrahedral mesh for cylinder pack and 2.493.229 tetrahedral mesh for rectangular pack due to the complexity of the model and it is enough for the stability of the numerical results. The mesh structures for the numerical models are shown in Fig. 3. The average skewness for both packs is 0.196.

The numerical analysis assumed the liquid RT44 to be an incompressible Newtonian fluid, and the buoyancy effect was modeled using Boussinesq's approximation. The other physical properties of the material were assumed constants, except for the thermal conductivity of RT44 (or composite). Thermal conductivity was measured experimentally and piecewise-linear profiles were created based on the temperature measurements. For each cell, the governing equations were solved numerically. Continuity, momentum, and energy equations, respectively;

$$\frac{\partial p}{\partial t}+\nabla\cdot\left(\rho\vec{V}\right)=0\,, \tag{2}$$

$$\rho\frac{\partial\vec{V}}{\partial t}+\rho\left(\vec{V}\cdot\nabla\right)\vec{V}=-\nabla P+\mu\nabla^2\vec{V}+\rho\beta\vec{g}\left(T-T_{ref}\right)+\vec{S}\,, \tag{3}$$

$$\frac{\partial}{\partial t}(\rho H)+\nabla\cdot\left(\rho\vec{V}H\right)=\nabla\cdot(k\nabla T)+S \tag{4}$$

where ρ is the density of the liquid RT44 (or GNP/RT44) and is the momentum source term. The enthalpy was expressed as the sum of the sensible enthalpy (h) and the latent heat (ΔH).

$$H=h+\Delta H\,, \tag{5}$$

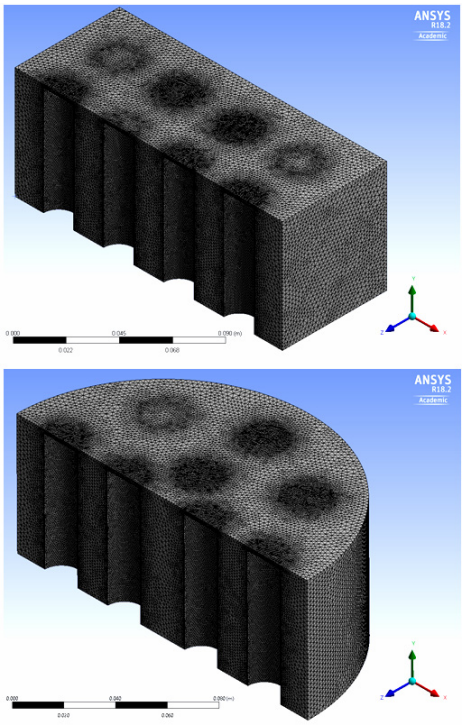

Fig. 3. The mesh structure of rectangular and cylinder packs.

$$h=h_{ref}+\int_{T_{ref}}^{T}cdT\,, \tag{6}$$

$$\Delta H=\gamma L \tag{7}$$

where h_{ref} is the enthalpy at the reference temperature, L is the latent heat, γ is the liquid fraction of material and it is calculated as follows:

$$\begin{aligned}&\gamma=0, && T<T_{om}\\ &\gamma=(T-T_{om})/(T_{em}-T_{om}), && T_{om}<T<T_{em}\\ &\gamma=1, && T>T_{em}\end{aligned}\,. \tag{8}$$

Here, γ = 0 represents the solid phase, γ between 0 and 1 represents mushy zone and γ = 1 represents the liquid phase. T_{om} and T_{em} are the onset melting and endset melting temperatures obtained from DSC tests.

3. Results and discussions

3.1 Thermophysical properties

The effect of 7 % GNP mass fraction, added into RT44 to increase thermal conductivity, on thermal properties is given in Table 1. Thermal conductivity measurements were carried out at 20 °C for the solid phase and 50 °C for the liquid phase within the air conditioning device. With the addition of GNP mass, 3.3 times enhancement was achieved in the solid phase and 2.3 times in the liquid phase.

As seen in Fig. 4, it was determined that the DSC curves showed similar behavior, but there was a decrease in the peak

Table 1. The measured properties of RT44 and 7 % GNP/RT44.

Material	T_{om} (°C)	T_{em} (°C)	$k_{@20\,°C}$ (W/mK)	$k_{@50\,°C}$ (W/mK)	H_m (J/g)	μ (kg/ms)
RT44	40.22	44.70	0.364	0.153	239.6	0.0082
7 % GNP/RT44	40.29	44.92	1.192	0.357	221.5	0.033

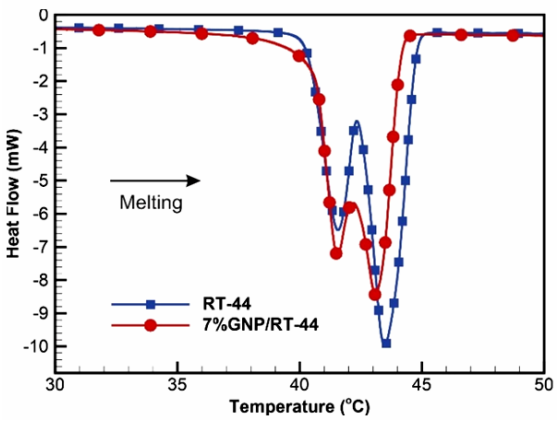

Fig. 4. DSC curves of RT44 and 7% GNP/RT44.

amplitude due to the nanoparticle addition. The analysis results of the DSC curves are given in Table 1 and it was determined that the melting onset (T_{om}) and melting endset temperatures (T_{em}) are not affected by the GNP mass fraction. On the other hand, the latent heat of melting (H_m) decreases in proportion to the decrease in the peak amplitude. Similarly, viscosity measurements show that 7 % nanoparticle addition has a negative effect on RT44 viscosity. The nanoparticle addition causes a 7.5 % capacity loss at the latent melting heat, while it causes 4 times to increase in viscosity. Although the capacity loss in the latent heat of melting is tolerable, an increase in the viscosity causes significant effects on the heat transfer mechanism in the melt phase.

3.2 Battery pack shape effect

The validation of the numerical studies was performed in a rectangular package for RT44 and a cylindrical package for 7 % GNP/RT44 by comparing with the related experimental data. As seen in Fig. 5, the temperature-time variation trend was similar for experimental and numerical cases at different measurement points.

With the initiation of the phase change, a small difference occurred in the trend of the experimental and numerical data. In the numerical analysis, the temperature remains constant during the phase change with the acceptance of RT-44 as a pure substance. In reality, the purity of paraffin wax type organic materials is degraded by adding some supporting materials to provide desired properties. This fact causes a slight difference in numerical and experimental analysis results during phase change. The same reason is true for difference between experimental and numerical results of 7 % GNP/RT-44. Although a small discrepancy (< 5 %) was seen during the phase change process, it can be said that numerical results are compatible with the experimental results.

The effects of battery pack shape on thermal responses are compared in Fig. 6 for all discharge rates. In fact, more heat accumulation occurs in the middle region of the cylinder pack.

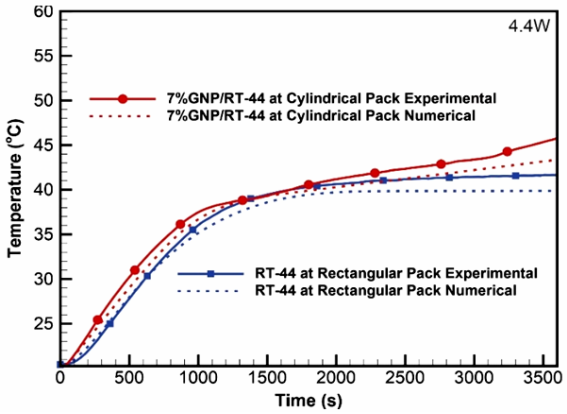

Fig. 5. The validation of numerical results with experimental results.

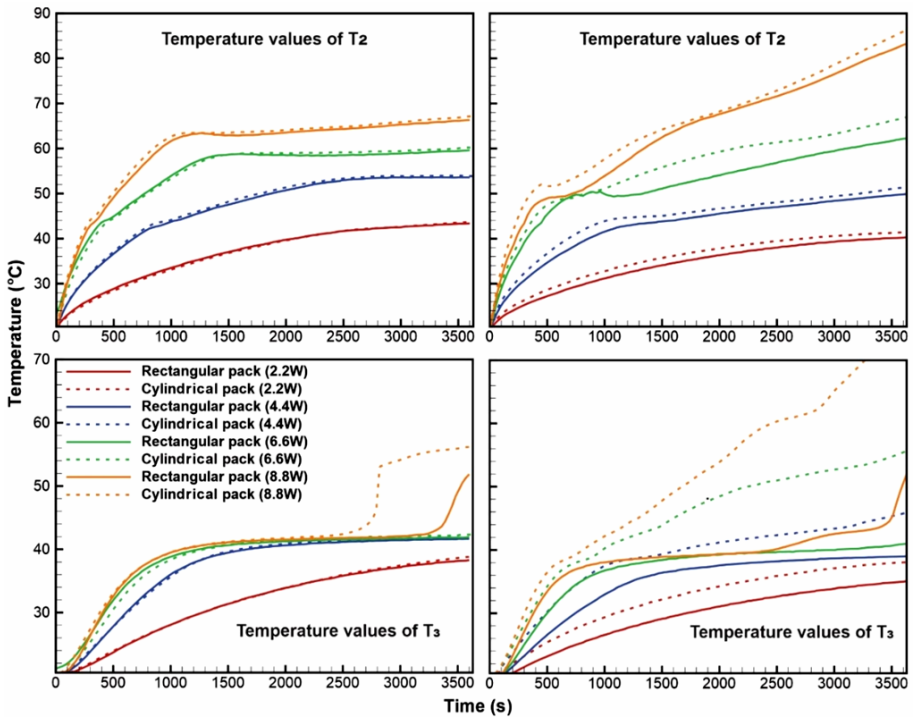

Fig. 6. Experimental thermal response comparison between rectangular and cylindrical pack.

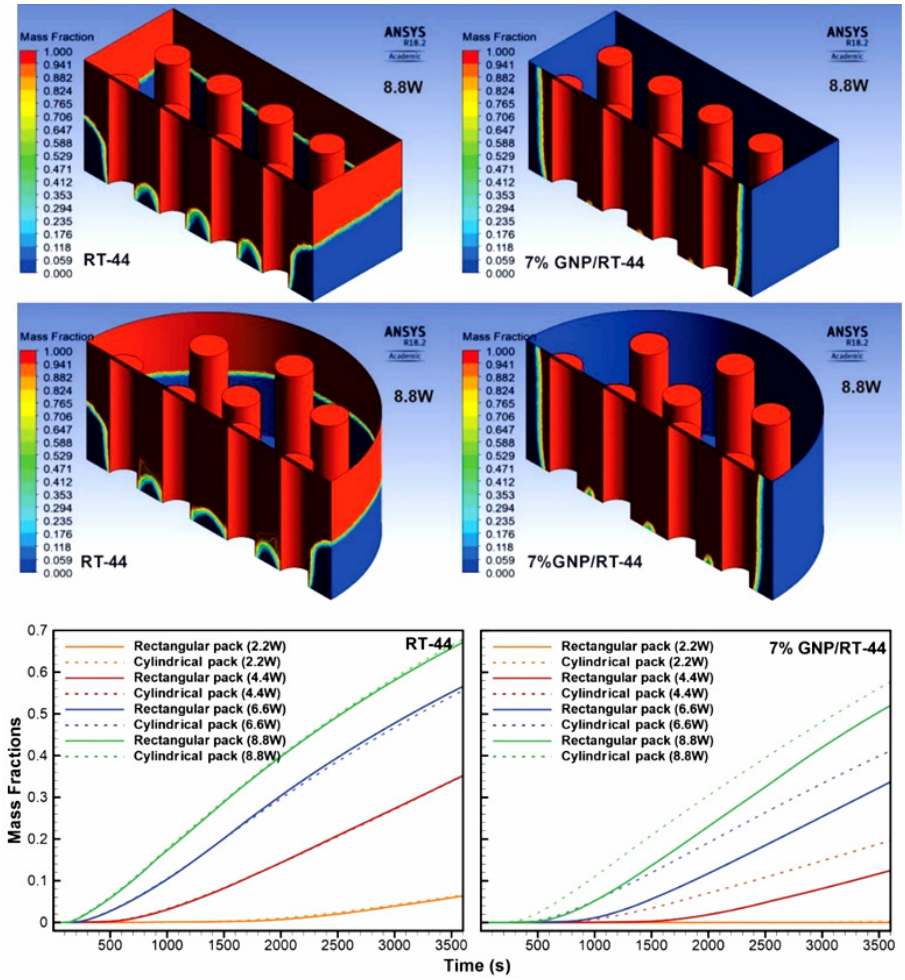

Fig. 7. The liquid fractions contours for different battery packs and liquid fractions variation with time.

This is evident from the earlier temperature rise of the T_3 (at 8.8 W) after the constant temperature behavior caused by natural convection in the cylinder pack compared to the rectangular one. Although the packs have the same volume and heat transfer surface, the more accumulation in the cylinder pack is due to the longer heat transfer path to dissipate it. The experimental thermal response comparisons were carried out on the cell in the inner region of the pack, where the maximum temperature ($T_{max} = T_2$) occurred. However, the maximum temperature responses were determined to be independent of the battery pack shape at the RT44 passive thermal protection system. The first reason is that the accumulated heat in the middle region of both packs cannot be dissipated effectively due to the low thermal conductivity of RT44. Another reason is the remaining of temperature as constant for a certain time period due to buoyancy-driven natural convection flows in the liquid phase of RT44. On the other hand, the battery pack shape creates some evident differences on the maximum temperature responses of the 7 % GNP/RT44 passive thermal protected system. During the discharge process, the time averaged temperature differences of the mutual points between the two battery packs ($T_{2\ av,\ cy}$ -$T_{2\ av,rec}$) were measured as 1.7 °C, 2.5 °C, 5.3 °C and 4.4 °C for 2.2 W, 4.4 W, 6.6 W and 8.8 W, respectively.

This difference is due to the reasons listed below: i) The deterioration of natural convection currents due to the increased viscosity in the liquid phase leads to a tendency of continuous increase in temperature; ii) The accumulated heat in the middle of the pack is better dissipated in the rectangular pack due to the increased heat conduction coefficient. This is evident from the fact that T_3 temperatures remain lower in the rectangular pack. The primary purpose of thermal protection of battery packs is to keep the maximum temperature as low as possible. According to these results, it can be said that the rectangular pack performs better than the cylindrical one. Fig. 7 gives the numerical results of liquid fraction contours at the end of the 3600 seconds for different battery packs operating at a discharge rate of 8.8 W. It also includes the formation of the liquid fraction through the time period of 3600 seconds. The liquid volume fraction-time variation for both packs is almost the same in the use of RT44 based thermal protection. In the rectangular pack of RT44, the volume liquid fractions at the end of 3600 seconds were measured as 6.3 %, 35.2 % 56.6 % and 67.3 % for 2.2 W, 4.4 W, 6.6 W and 8.8 W, respectively. The melt front starts around the cells and reaches the upper half of

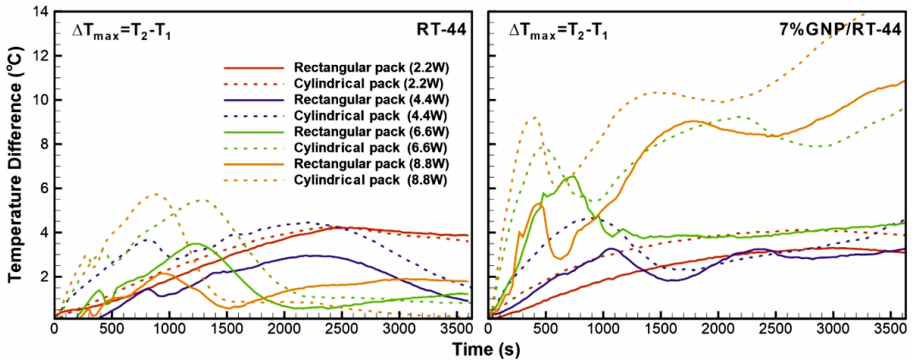

Fig. 8. The maximum temperature difference response of different battery packs.

the outer wall for the two pack systems. This is the result of buoyancy-driven flows occurring within the liquid RT44. On the other hand, the high viscosity of the liquid 7 % GNP/RT44 composite significantly restricts the melt front movement by weakening the buoyancy flows. Such that the liquid fractions of 7 % GNP/RT44 that starts around the cells expand over time but cannot reach the outer walls of the packs at the end of the 3600 seconds. As a result, less melting occurs when using 7 % GNP/RT44 for both pack systems compared to RT44. Additionally, 7 % GNP/RT44 thermal protection behaves differently in terms of the melting fraction at the rectangular and cylindrical packs. The liquid volume fractions in rectangular pack at the end of 3600 seconds were measured as 0.05 %, 12.5 %, 33.7 % and 52.0 % for 2.2 W, 4.4 W, 6.6 W and 8.8 W, respectively. On the other hand, in the cylindrical pack, they increases slightly and are measured as 0.3 %, 19.7 %, 41.2 % and 57.7 % for 2.2 W, 4.4 W, 6.6 W and 8.8 W, respectively. Because, as mentioned before, more heat accumulation occurs in the middle of the cylindrical pack.

The maximum temperature difference (ΔT_{max}) inside the battery pack can be determined as:

$$\Delta T_{max} = T_2 - T_1 \tag{9}$$

where T_2 is the inner and the maximum temperature of the battery pack, T_1 is the outer and minimum temperature of the battery pack. The effect of the battery pack shape on the experimental response of the ΔT_{max} is given in Fig. 8. The battery pack shape creates significant differences in the ΔT_{max} in both RT44 and 7 % GNP/RT44 based passive thermal protection.

For example using 7 % GNP/RT44, the average differences between two battery packs ($\Delta T_{max,cy}$ - $\Delta T_{max,rec}$) determined as 0.9 °C, 0.8 °C, 3.5 °C, and 2.8 °C, respectively, for 2.2 W, 4.4 W, 6.6 W, and 8.8 W during discharge. The higher ΔT_{max} in the cylinder pack is the result of more heat accumulation in the interior region and less heat transfer to the outside of the pack.

3.3 Low to high discharge rate thermal responses of rectangular pack

As a first design criterion, the maximum temperature-time

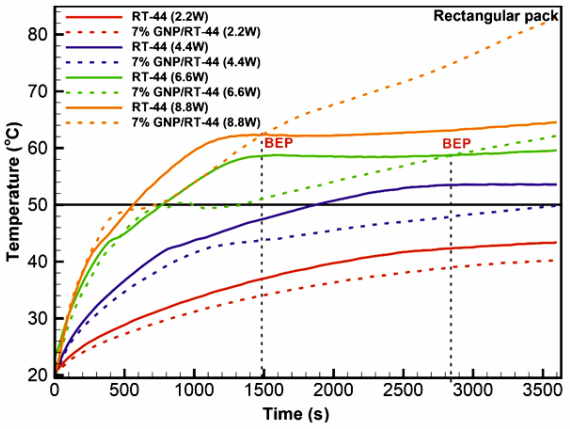

Fig. 9. The comparison of the maximum temperature responses for RT44 and 7 % GNP/RT44.

variation in the rectangular battery pack is compared in Fig. 9 for RT44 and 7 % GNP/RT44. In cases where melting was provided, thermal responses created four different stages for RT44 (and 7 % GNP/RT44). Before the melting process at stage 1 (S_1), the maximum temperature of the battery (T_2), rises quickly depending on the discharging rates. However, at 2.2 W and lower discharge rates, thermal equilibrium is achieved before reaching the melting temperature due to the storage of generated heat by the RT44 (or 7 % GNP/RT44) medium and transferring some part of it to the outside of the pack by convection. In other words, thermal responses of the battery pack consist of entirely the S_1 during the discharge at 2.2 W. At S_1, heat transfer takes place entirely by conduction, and thermal responses of the battery pack are significantly reduced due to more heat penetration to the medium depending on the increase of thermal conductivity coefficient in 7 % GNP/RT44. The decrease in thermal responses is an essential enhancement in limiting the maximum temperature of the battery packs, but it is seen that the degree of it decreases as the discharge rate increases. In the second stage (S_2), the heat transfer mechanism is also heat conduction, and the rate of temperature increase is reduced depending on the initialization of the melting of RT44. It is observed that S_2 becomes shorter, and the slope of it increases directly proportionally depending

on the increase of the discharge rates. A similar consideration applies to 7 % GNP/RT44, which provides a lower temperature rise due to increased thermal conductivity compared to RT44 at a discharge rate of 4.4 W. However, it appears that the S_2 thermal responses of 7 % GNP/RT44 thermal protection are roughly the same as the RT44 for 6.6 W and worse for 8.8 W. The reason for this is that in 7 % GNP/RT44 with higher thermal conductivity, the rapid liquid layer is formed around the cells, especially at high discharge rates. As given in Table 1, the thermal conductivity in the liquid state drops significantly due to low molecular order. At the third stage (S_3), evident constant temperature plateaus occur for the RT44 at discharge rates equal to and higher than 4.4 W. The reason for this is that when the liquid RT44 around the cells reaches a certain thickness, the convective heat transfer mechanism becomes dominant under the effect of significant buoyancy forces. Also, constant temperature plateaus occur at higher temperatures and shorter duration due to increased discharge rates. The constant temperature values were measured at approximately 53.5 °C, 58.5 °C and 62.1 °C for the discharge rates of 4.4 W, 6.6 W and 8.8 W, respectively. Especially at high discharge rates, it may be a control advantage to reduce the constant temperature plateaus below 50 °C, the critical temperature for battery pack thermal protection. In the use of 7 % GNP/RT44 composite, this event seems to have been achieved exactly and the constant temperature plateaus occur around 50 °C again. As mentioned above, rapid liquid formation around the cells adjusts the constant plateaus to a lower temperature. However mentioned advantageous situation does not continue for a long time, and the S_3 ends in a very short time compared to RT44. Because the convective flows that started in the narrow liquid region around the battery cells are slowed down due to the increasing viscosity as the liquid region begins to expand. As given in Table 1, the RT44 viscosity value increases from 0.008 Pa.s to 0.033 Pa.s after 7 % GNP addition. In 7 % GNP/RT44 passive thermal protection, it is seen that the temperature starts to increase again with a significant slope as the conduction starts to become dominant again. The next stage (S_4) in 7 % GNP/ RT44 passive thermal protection occurs when the temperature begins to rise again with a significant gradient due to the conduction dominant heat transfer mechanism. On the other hand, it was observed that S_4 in RT44 protection started after a large amount of PCM melting and the slope of temperature increase was negligible small due to the ongoing convection dominant heat transfer. Performance evaluation in terms of preventing the maximum temperature increase is explained below and given in Table 2.

Both RT44 and 7 % GNP/RT44 have managed to keep the maximum temperature below 50 °C at low discharge rates (2.2 W). At low to moderate discharge rates (2.2 W-4.4 W), the maximum temperature of the battery has been kept lower throughout the entire discharge process using GNP. The effective protection time (t_{eff}) can be defined as the time that the maximum temperature of the battery pack remains below 50 °C.

Table 2. The performance evaluation of RT44 and 7 %GNP/RT44.

Tmax (°C) at 3600 s			t_{eff} (sec)	
Discharge rate	RT44	7 % GNP/RT44	RT44	7 % GNP/RT44
2.2 W	43.4	40.2	-	-
4.4 W	53.6	49.8	1870.7	3662.5
6.6 W	59.6	62.2	769.7	1334.0
8.8 W	64.5	83.0	561.3	718.4

The enhancement in the effective protection time performance over RT-44 can be calculated from the following expression;

$$\%\,t_{eff} = \left(\frac{t_{eff,GNP/RT44} - t_{eff,RT44}}{t_{eff,RT44}} \right) * 100 \,. \tag{10}$$

At moderate discharge rate (4.4 W), 7 % GNP/RT44 provided effective protection (T_{max} < 50 °C) for 3662.5 seconds, while RT44 was able to achieve this for 1870.7 seconds. In other words, 7 % GNP/RT44 thermal protection extends the effective protection time by 95.8 % compared to RT44. The effective protection times of both RT44 and 7 % GNP/RT44 are considerably shortened at high discharge rates. However, 7 % GNP/RT44 is still successful in extending protection time more effectively, but this efficiency is steadily decreasing. The efficiency of extending protection time decreases from 73.3 % (6.6 W) to 28.0 % (8.8 W) compared to RT44. Thermal protection based on the use of GNP nanoparticles at high discharge rates keeps the maximum temperature lower than RT44 protection up to a break-even point (BEP), but the situation reverses completely after this point. BEP occurs at 58.7 °C (t = 2845 s) for 6.6 W discharge rate and 62.3 °C (t = 1490 s) for 8.8 W discharge rate. The temperature of T_2 remains almost constant on the RT44 for 6.6 W and 8.8 W discharge rates, while it increases with a significant slope at 7% GNP/RT44. At the end of the discharge period of 6.6W, T_2 temperatures were measured as 59.6 °C and 62.2 °C for RT44 and 7 % GNP/RT44, respectively. They reach the values of 64.5 °C and 83.0 °C at the end of the 8.8 W discharge period.

As stated before, the second design criterion for battery packs is to keep the maximum temperature difference within it below 5 °C. The maximum temperature difference-time variation in the rectangular battery pack is compared in Fig. 10 for RT44 and 7 % GNP/RT44. Initially, the maximum temperature difference between critical cells continuously increases until melting begins. The formation of a constant temperature plateau in the inner region of the battery pack after melting causes a significant decrease in maximum temperature differences. Because, while the temperature in the inner region remains constant, that in the outer region is still increasing. How long this decrease will continue depends entirely on the continuity of the constant temperature plateau. It is seen that the maximum temperature difference in passive thermal protection of RT44 easily provides the desired design criterion (< 5 °C). Although it

is shortened due to the increase of the discharge rate, the relatively long duration of the constant temperature plateau causes the maximum temperature difference to decrease significantly. On the other hand, at 7 % GNP/RT44 passive thermal protection, the shorter constant temperature plateau and almost disappearance of it as the discharge rate increases provide worse protection in terms of the maximum temperature difference. Especially at high discharge rates (6.6 W and 8.8 W), it is seen that the maximum temperature difference exceeds 5 °C in 7 % GNP/RT44 passive thermal protection. The temperature difference along cell height was obtained by plotting the thermal responses obtained experimentally from thermocouples placed in the lower point (T_4) and upper point (T_6) of the one specified cell according to time (Fig. 11). This figure also includes numerically obtained temperature contours at the instant of 3600 s. Experimental thermal responses obtained using passive thermal protection based on RT44 show that the upper region of the cell is warmer than the lower region and a significant temperature difference occurs across the cell. This result is also consistent with temperature contours obtained from numerical analysis. Considering the temperature contours, it is seen that more uniform temperature distribution is formed on the cells at 7 % GNP/RT44 thermal protection. In RT44, buoyancy currents create a sharp temperature variation from low to high between the lower and upper regions of each cell, respectively. On the other hand, a more uniform temperature distribution occurs in 7 % GNP/RT-44 due to the suppression of buoyancy currents by the increasing viscosity with the addition of nanoparticles.

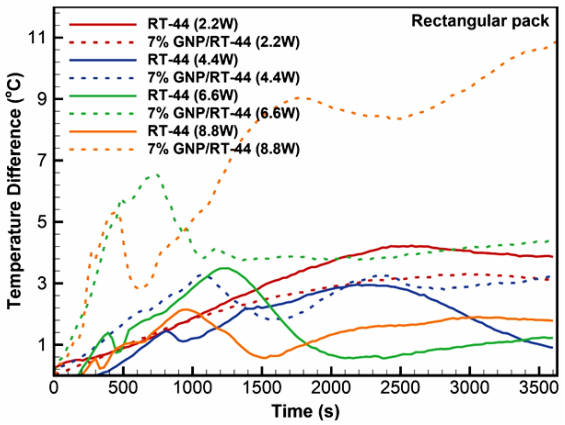

Fig. 10. The comparison of the maximum temperature difference responses for RT44 and 7 % GNP/RT44.

The experimental temperature difference especially in the upper and lower region of the cell increases in proportion to the discharge rates. After 3600 seconds, temperature differences were measured as 2.52 °C, 3.95 °C, 5.68 °C and 7.44 °C for 2.2 W, 4.4 W, 6.6 W and 8.8 W discharge, respectively. Only in battery packs based on RT44 passive thermal protection, the temperature difference along cell height can be made uniform

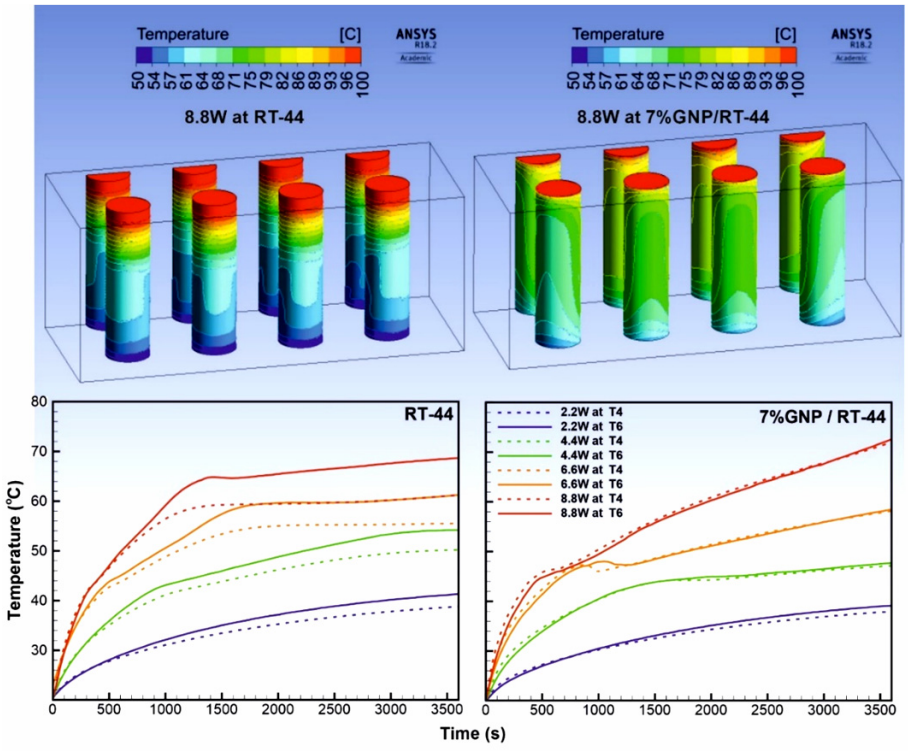

Fig. 11. Temperature contours and temperature responses throughout the cell.

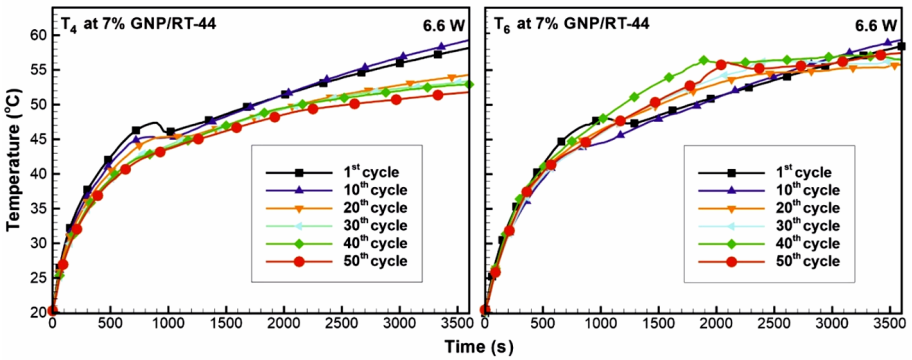

Fig. 12. The stability of 7 % GNP/RT44 composites.

by using variable size fins. Because the heat transfer rate increases with the addition of fins and the highest heat transfer rate are obtained in the double-fin configuration for the semi-circular cylinder [35, 36]. On the other hand, in passive thermal protection based on the use of 7 % GNP/RT44, there is no significant temperature difference along with the cell height. A more uniform temperature distribution can also be seen from the temperature contours. The first reason is the better penetration of the heat released from the cells into the material due to the enhanced thermal conductivity. The second reason is the suppression of buoyancy flows due to the GNP additive increasing the viscosity in the liquid phase.

To determine the stability of GNP nanoparticles within the RT44 subjected to high discharge rate (6.6 W), the thermal responses at the end of different melting/solidification cycles were compared for the measurement points of the T_4 and T_6 (Fig. 12). Melting/solidification cycles were carried out in-situ to ensure complete melting and solidification. Unfortunately, it has been observed that nanoparticles settled down to the bottom of the pack with complete melting at high discharge rates. As a result, the pack was divided into two separate regions as the upper part mostly RT44 and the lower part GNP weighted RT44. As the number of melting/solidification cycles increases, further improvement is achieved in the thermal response of the bottom cell region (at T_4) depending on the GNP concentration increase. However, a behavior similar to the typical RT44 thermal response was observed in the upper cell region. It is seen that thermal response (T_6) in the upper part of the cell worsens primarily after phase change, depending on the number of cycles, but then improves with the formation of a constant temperature plateau.

Thermal performance evaluations at low to high discharge rates show that both RT44 and 7 % GNP/RT44 have some advantages or disadvantages against each other in different stages of the discharge process in battery pack protection. The disadvantages of both passive thermal protection methods still have to be eliminated for effective thermal protection.

4. Conclusions

In this study, the effects of battery pack shape on the performance of PCM (or GNP/PCM) passive thermal protection systems were investigated. Also, from low to high discharge rates thermal performance of the thermally enhanced PCM composite (GNP added) was compared with passive thermal protection with PCM only. The following conclusions are drawn.

It has been determined that the cylinder pack performs worse than the rectangular pack in terms of the maximum temperature and maximum temperature difference performance criteria for the battery pack. The longer heat transfer path of the cylinder pack causes more heat accumulation in the middle region and thus more liquid volume fraction to be formed. The 7 % GNP/RT44 composite has been found to improve performance in conditions with a conduction-dominant heat transfer mechanism, such as pre-melting and early melting, compared to RT44. On the other hand, it causes worse performance due to the loss of thermal plateau advantage due to deteriorating convective flow movements in the case of sufficient liquid fraction. In other words, the GNP/RT44 composite only performs better up to the breakeven point. While RT44 creates a temperature difference in the upper and lower part of the cell due to buoyancy movements, 7 % GNP/RT44 creates a more homogeneous temperature distribution. The complete melting/solidification cycles at high discharge rates showed that the homogeneous distribution of nanoparticles in RT44 was disturbed by sedimentation.

Future studies should be carried out to improve the stability of nanoparticles in the PCM without disturbing the improvement in thermal conductivity. It is necessary also to limit the fraction of nanoparticles that suppress convective currents due to the undesired increase in viscosity. The thermal plateau seen in the RT44 can be transformed into a control advantage by lowering its temperature. The finned structures can be added around the cells to achieve uniform temperature throughout the cell height.

Nomenclature

W	: Heat power (W)
T	: Temperature (°C)
k	: Thermal conductivity (W/mK)
h	: Latent heat (J/g)

μ : Dynamic viscosity (kg/ms)
V : Velocity (m/s)
P : Pressure (Pa)
β : Thermal expansion coefficient
g : Gravitational acceleration (m/s^2) subscripts
om : Onset melting
em : Endset melting
max : Maximum
m : Melting
eff : Effective protection
av : Average
rec : Rectangle
cy : Cylinder
ref : Reference

Acronyms

PCM : Phase change material
GNP : Graphene nanoplatelets
EG : Expanded graphite
DSC : Differential scanning calorimetry
S : Stage
EV : Electrical vehicle
HEV : Hybrid electrical vehicle

References

[1] A. Jarrett and I. Y. Kim, Design optimization of electric vehicle battery cooling plates for thermal performance, *Journal of Power Sources*, 196 (23) (2011) 10359-10368.

[2] C. Lin, S. Xu, G. Chang and J. Liu, Experiment and simulation of a LiFePO4 battery pack with a passive thermal management system using composite phase change material and graphite sheets, *Journal of Power Sources*, 275 (2015) 742-749.

[3] E. Gümüşsu, Ö. Ekici and M. Köksal, 3-D CFD modeling and experimental testing of thermal behavior of a Li-Ion battery, *Applied Thermal Engineering*, 120 (2017) 484-495.

[4] Y. S. Ranjbaran, S. J. Haghparast and M. H. S. G. R. Molaeimanesh, Numerical evaluation of a thermal management system consisting PCM and porous metal foam for Li-ion batteries, *Journal of Thermal Analysis and Calorimetry*, 141 (5) (2020) 1717-1739.

[5] H. Yang, H. Zhang, Y. Sui and C. Yang, Numerical analysis and experimental visualization of phase change material melting process for thermal management of cylindrical power battery, *Applied Thermal Engineering*, 128 (2018) 489-499.

[6] J. P. Hadiya and A. K. N. Shukla, Experimental thermal behavior response of paraffin wax as storage unit, *Journal of Thermal Analysis and Calorimetry*, 124 (3) (2016) 1511-1518.

[7] N. O. Moraga, J. P. Xamán and R. H. Araya, Cooling Li-ion batteries of racing solar car by using multiple phase change materials, *Applied Thermal Engineering*, 108 (2016) 1041-1054.

[8] J. Yan, Q. Wang, K. Li and J. Sun, Numerical study on the thermal performance of a composite board in battery thermal management system, *Applied Thermal Engineering*, 106 (2016) 131-140.

[9] J. Chen, S. Kang, J. E, Z. Huang, K. Wei, B. Zhang, H. Zhu, Y. Deng, F. Zhang and G. Liao, Effects of different phase change material thermal management strategies on the cooling performance of the power lithium ion batteries: a review, *Journal of Power Sources*, 442 (2019) 227228.

[10] S. A. Hallaj and J. R. Selman, A novel thermal management system for electric vehicle batteries using phase-change material, *Journal of The Electrochemical Society*, 147 (9) (2000) 3231.

[11] W. Ye, Enhanced latent heat thermal energy storage in the double tubes using fins, *Journal of Thermal Analysis and Calorimetry*, 128 (1) (2017) 533-540.

[12] F. Bahiraei, A. Fartaj and G. A. Nazri, Experimental and numerical investigation on the performance of carbon-based nanoenhanced phase change materials for thermal management applications, *Energy Conversion and Management*, 153 (2017) 115-128.

[13] S. A. Khateeb, M. M. Farid, J. R. Selman and S. A. Hallaj, Design and simulation of a lithium-ion battery with a phase change material thermal management system for an electric scooter, *Journal of Power Sources*, 128 (2) (2004) 292-307.

[14] P. Ping, R. Peng, D. Kong, G. Chen and J. Wen, Investigation on thermal management performance of PCM-fin structure for Li-ion battery module in high-temperature environment, *Energy Conversion and Management*, 176 (2018) 131-146.

[15] Z. Wang, H. Zhang and X. Xia, Experimental investigation on the thermal behavior of cylindrical battery with composite paraffin and fin structure, *International Journal of Heat and Mass Transfer*, 109 (2017) 958-970.

[16] S. A. Khateeb, S. Amiruddin, M. Farid, J. R. Selman and S. Al-Hallaj, Thermal management of Li-ion battery with phase change material for electric scooters: experimental validation, *Journal of Power Sources*, 142 (2005) 345-353.

[17] Z. Rao, Y. Huo, X. Liu and G. Zhang, Experimental investigation of battery thermal management system for electric vehicle based on paraffin/copper foam, *Journal of the Energy Institute*, 88 (3) (2015) 241-246.

[18] R. Zhao, J. Gu and J. Liu, Optimization of a phase change material based internal cooling system for cylindrical Li-ion battery pack and a hybrid cooling design, *Energy*, 135 (2017) 811-822.

[19] A. Mills and S. A. Hallaj, Simulation of passive thermal management system for lithium-ion battery packs, *Journal of Power Sources*, 141 (2005) 307-315.

[20] G. Jiang, J. Huang, M. Liu and M. Cao, Experiment and simulation of thermal management for a tube-shell Li-ion battery pack with composite phase change material, *Applied Thermal Engineering*, 120 (2017) 1-9.

[21] U. N. Temel and B. Y. Çiftçi, Determination of thermal properties of A82 organic phase change material embedded with different type nanoparticles, *Journal of Thermal Science and Technology*, 38 (2) (2018) 75-85.

[22] L. W. Fan, X. Fang, X. Wang, Y. Zeng, Y. Q. Xiao, Z. T. Yu, X. Xu, Y. C. Hu and K. F. Cen, Effects of various carbon nanofillers on the thermal conductivity and energy storage properties of paraffin-based nanocomposite phase change materials, *Applied Energy*, 110 (2013) 163-172.

[23] A. Babapoor, M. Azizi and G. Karimi, Thermal management of a Li-ion battery using carbon fiber-PCM composites, *Applied Thermal Engineering*, 82 (2015) 281-290.

[24] X. Tong, D. Q. Peng, S. Y. Wu, C. D. Nie, Z. Q. Wang and S. G. Gong, The effects of various carbon nanofillers on the thermal properties of paraffin for energy storage applications, *Journal of Thermal Analysis and Calorimetry*, 124 (1) (2015) 181-188.

[25] U. N. Temel, K. Somek, M. Parlak and K. Yapici, Transient thermal response of phase change material embedded with graphene nanoplatelets in an energy storage unit, *Journal of Thermal Analysis and Calorimetry*, 133 (2) (2018) 907-918.

[26] X. Duan and G. F. Naterer, Heat transfer in phase change materials for thermal management of electric vehicle battery modules, *International Journal of Heat and Mass Transfer*, 53 (2010) 5176-5182.

[27] Z. Wang, H. Zhang and X. Xia, Experimental investigation on the thermal behavior of cylindrical battery with composite paraffin and fin structure, *International Journal of Heat and Mass Transfer*, 109 (2017) 958-970.

[28] Z. Ling, J. Chen, X. Fang, Z. Zhang, T. Xu, X. Gao and S. Wang, Experimental and numerical investigation of the application of phase change materials in a simulative power batteries thermal management system, *Applied Energy*, 121 (2014) 104-113.

[29] P. Goli, S. Legedza, A. Dhar, R. Salgado, J. Renteria and A. A. Balandin, Graphene-enhanced hybrid phase change materials for thermal management of Li-ion batteries, *Journal of Power Sources*, 248 (2014) 37-43.

[30] Z. Ling, F. Wang, X. Fang, X. Gao and Z. Zhang, A hybrid thermal management system for lithium ion batteries combining phase change materials with forced-air cooling, *Applied Energy*, 148 (2015) 403-409.

[31] M. A. Abdelatief, A. A. Zamel and S. A. Ahmed, Elliptic tube free convection augmentation: an experimental and ANN numerical approach, *International Communications in Heat and Mass Transfer*, 108 (2019) 104296.

[32] M. A. Abdelatief and M. A. Omara, Free convection experimental study inside square tube with inner roughened surface at various inclination angles, *International Journal of Thermal Sciences,* 144 (2019) 11-20.

[33] J. P. Holman, *Experimental Methods for Engineers*, 7th Ed., McGraw-Hill, New York (2011).

[34] ANSYS, *ANSYS Fluent User's Guide, Release 18.2*, ANSYS Inc. (2016).

[35] M. L. Elsayed, M. A. Abdelatief, S. A. Ahmed, M. S. Emeara and W. M. Elwan, Thermal design evaluation of ribbed/grooved tubes: an entropy and exergy approach, *International Communications in Heat and Mass Transfer,* 120 (2021) 105048.

[36] A. A. Abdelfattah, E. Z. Ibrahim, S. A. E. S. Ahmed, W. M. Elwan, M. L. Elsayed and M. A. Abdelatief, Thermal performance augmentation of a semi-circular cylinder in crossflow using longitudinal fins, *International Communications in Heat and Mass Transfer,* 125 (2021) 105159.

Ümit Nazlı Temel received his Ph.D. degree from the Sivas Cumhuriyet University in 2013. Currently he is an Assistant Professor in the Department of Mechanical Engineering. His main working areas are thermal management, phase change materials, fluid flow, particle image velocimetry.

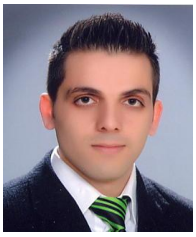

Ferhat Kilinc received his Ph.D. degree from the Sivas Cumhuriyet University in 2015. Currently he is an Assistant Professor in the Department of Mechanical Engineering. His main working areas are heat transfer in nanofluids, heat exchangers, heat insulation, thermal imaging, thermal management, PCMs.